Journal of the European Ceramic Society 22 (2002) 573–578

www.elsevier.com/locate/jeurceramsoc

Electrical conductivity control in uranium-doped $PbZrO_3$–$PbTiO_3$–$Pb(Mg_{1/3}Nb_{2/3})O_3$ pyroelectric ceramics

S.B. Stringfellow[a], S. Gupta[b], C. Shaw[a], J.R. Alcock[a,*], R.W. Whatmore[a]

[a]*School of Industrial and Manufacturing Science, Cranfield University, Bedford MK43 0AL, UK*
[b]*Laser Materials Division, Centre for Advanced Technology, Indore 452013, India*

Received 24 January 2001; received in revised form 11 April 2001; accepted 28 April 2001

Abstract

The effects of uranium doping on the electrical conductivity and pyroelectric/dielectric properties of lead zirconate–lead titanate–lead magnesium niobate (PZ–PT–PMN) ferroelectric ceramics have been investigated. These ceramics have the general formula $Pb_{1.01}\{(Mg_{1/3}Nb_{2/3})_{0.025}(Zr_{0.825}Ti_{0.175})_{0.975}\}_{1-z}U_zO_3$ (Whatmore, R.W., UK Patent GB2347416A, 2001). Good pyroelectric properties have been obtained for this system, with a pyroelectric coefficient of 3×10^{-4} Cm^{-2} K^{-1} at $z=0.006$, and corresponding pyroelectric figures of merit of $F_V=0.066$ m^2 C^{-1} and $F_D=4.7\times10^{-5}$ $Pa^{-1/2}$. It was found that the DC resistivity varied from 1.2×10^{10} Ωm for $z=0.0048$ to 1×10^8 Ωm for $z=0.0145$ in a highly predictable fashion, such that the DC conductivity/doping law was accurately described by the equation: $\sigma_o=A\exp(-\alpha a z^{-1/3}-E_a/kT)$ with $\alpha=0.63$ $Å^{-1}$ and $E_a=0.28\pm0.04$ eV. This conductivity law corresponds very closely to that reported previously for uranium-doped ceramics in the lead zirconate–lead titanate–lead iron niobate system. This implied a similar conduction mechanism, probably hopping between non-ionised dopant ion sites. It is demonstrated that this relationship can be used as a predictive tool for electrical conductivity control in these systems.

Keywords: Electrical conductivity; Pervoskites; PMN; Pyroelectric properties, PZT

1. Introduction

Ferroelectric ceramics and single crystals have had widespread use in the field of pyroelectric infra-red radiation (IR) detection for many years.[1,2] Pyroelectric devices work by absorbing the IR energy in a thin slice of a polar dielectric (usually called the "element"). The charge released as a consequence of the resulting change in temperature is allowed to flow as a current in an external circuit. Usually, the element is connected to a high input impedance FET amplifier. Relative to semiconductor detectors of medium and long wavelength IR, these devices offer the advantages of low cost fabrication and broadband operation coupled with a performance adequate for many applications, especially in the consumer field. The physics of operation of such devices has been extensively studied[1] and reviewed[2,3] and figures of merit (FOM) have been defined[1–5] which describe the performance of pyroelectric detectors in terms of the physical properties of these materials:

$$F_V=\frac{p}{c'\varepsilon_0\varepsilon_r} \tag{1}$$

$$F_D=\frac{p}{(c'\varepsilon_0\varepsilon_r\tan\delta)^{\frac{1}{2}}} \tag{2}$$

where p is the pyroelectric coefficient, C is the specific heat capacity, ε_0 is permittivity of free space, ε_r is the relative permittivity of the material and $\tan\delta$ is the loss tangent.

F_V is proportional to the device voltage responsivity and F_D to its specific detectivity, assuming that circuit noise is dominated by the AC Johnson noise due to the AC conductance of the element. For circuits operated in voltage mode, F_D is the most important materials figure of merit.

Pyroelectric ceramics have many advantages over other established single crystal pyroelectrics such as lithium niobate or tryglycine sulphate (TGS). For example, it is

* Corresponding author.
E-mail address: j.r.alcock@cranfield.ac.uk (J.R. Alcock).

0955-2219/02/$ - see front matter
PII: S0955-2219(01)00316-8

relatively easy to produce large blocks of uniform material with no cleavage planes, and wafers of these materials are robust and can be processed with equipment similar to that used in the semiconductor industry. As a wide range of solid solution systems exist, there is ample opportunity to optimise the particular properties of interest. Lead zirconate titanate (PZT) is a notable example. With appropriate selection of composition and dopants it is possible to develop families of piezoelectric[6] and pyroelectric[7] materials for different sensor and actuator applications. A particularly successful system has been reported[8–11] which was based upon lead zirconate–lead titanate–lead iron niobate (PZ–PT–PFN). From Eqs. (1) and (2) it can be shown that the desired characteristics of any pyroelectric material are that it should have a low relative permittivity in the temperature range of use, low dielectric loss and a high pyroelectric coefficient. However, there are other important physical properties that can require control, particularly electrical resistivity. During operation, a pyroelectric device is required to generate charge in response to a change in the intensity of radiation incident on its surface. Very slow temperature changes can also give rise to a gradual build up of charge that can eventually cause the input of the following electronics to saturate. In the case of a single element detector, similar to those used in intruder alarms, a very high value resistor can be placed between the input gate of the FET and ground, effectively providing a means for charge to leak away.[3] A resistor in parallel with the pyroelectric element also fixes the RC circuit time constant, and hence the frequency response of the device. As devices get more complex and are engineered as two-dimensional (2D) arrays, it becomes impossible to physically build these large value resistors into the circuit. An alternative technique is to use a pyroelectric material with a controlled resistivity; effectively building the gate bias resistor into the detector element.

For the perovskite oxide group (with the general formula ABO_3), to which PZT belongs, doping the 'B' site with uranium has previously been used[12] to alter the resistivity and ageing characteristics of a morphotropic phase boundary composition of PZT. Whatmore and co-workers[8–11] reported the effects of uranium doping on the pyroelectric and resistive properties in the PZ–PT–PFN ceramic system. Their work on two quite different compostions[11] $Pb(Zr_{0.76}Fe_{0.10}Nb_{0.10}Ti_{0.04})O_3$ and $Pb(Zr_{0.68}Fe_{0.14}Nb_{0.14}Ti_{0.04})O_3$ confirmed the wide applicability of this dopant to control both resistivity and relative permittivity and loss.

The work reported here is part of a study that has looked at optimising another pyroelectric ceramic composition based on a solid solution of lead magnesium niobate–lead titanate–lead zirconate (PMN–PT–PZ) for infrared detector arrays. Ouchi et al.[13,14] reported the dielectric and piezoelectric properties of many compositions in this system, although they did not cover pyroelectric properties. Choi et al.[15] have reported the pyroelectric properties of compositions along the PMN–PT compositional line. Recent work[16] has investigated the pyroelectric properties of some compositions close to lead zirconate in this system. In the work reported here, one particular composition has been selected on the basis of the FOMs detailed above. The effects of uranium doping on its resistivity, dielectric and pyroelectric properties have been investigated.

2. Experimental procedure

The dielectric and pyroelectric properties of compositions in the solid solution system $Pb_{1+\delta}(Mg_{1/3}Nb_{2/3})_y(Zr_{(1-x)}Ti_x)_{(1-y)}O_3$ (PMNZT) have been examined, and a detailed assessment of these will be published elsewhere.[16] On the basis of these results, uranium doping of a base PMNZT composition was investigated, with the target of achieving a controllable room temperature DC resistivity, without excessively compromising its pyroelectric properties. The compositions investigated possessed the general formula:

$$Pb_{1.01}(Mg_{1/3}Nb_{2/3})_{0.025}(Zr_{0.825}Ti_{0.175})_{0.9751-z}U_zO_3$$

2.1. Powder preparation

The first stage of powder preparation was the reaction of magnesium carbonate and niobium pentoxide (Aldrich Chemical Company), to form the columbite–structured mixed-oxide magnesium niobate by the routes described previously.[17,18] The powders were ball milled in a polyethylene pot with water, 0.1% DISPEX® (Allied Colloids) as a dispersant and 10 mm diameter zirconia milling media for 18 h. After drying in an oven at 338 K for 24 h the powder was passed through a 300 μm sieve and then calcined in an alumina crucible at 1273 K for 4 h. The presence of the columbite phase was confirmed by XRD (Philips PW1720). The magnesium niobate was then milled with the remaining constituents lead (II) oxide (BDH, GPR) zirconium (IV) oxide (Aldrich $<5\mu m$), titanium (IV) oxide (Aldrich, 325 mesh) for a further 18 h in a 0.1% DISPEX® aqueous solution.

The milled powder was dried and sieved. It was then calcined at 1073 K for 6 h to form a single-phase material, confirmed by XRD (Philips PW1720). An aqueous binder, Glascol® (4% by weight) was added to the powder and using a combination of ultrasonics and high shear mixing (Silverson) agglomerates were broken up during binder addition. The final slurry was dried in an oven at about 350 K. The powder was sieved through a 70 μm sieve prior to pressing 8 g lots in a 30 mm die at 126 MPa.

2.2. Sample preparation

The pellets were de-bound at 873 K for 5 min, and then sintered at 1523 K for 45 min. Sample pellets were weighed after de-binding to determine the initial green density and the weight loss. During sintering the pellets were separated by platinum foil and covered with a close fitting alumina crucible. After sintering the pellets were weighed and measured to determine their bulk densities. Typically the samples were 26 mm in diameter and 2 mm thick. Sample densities were all higher than 98% of theoretical density. Average grain size was approximately 5 μm. Prior to electrode deposition the faces of the sintered discs were ground flat with a final surface finish of 3000 grit. Two types of electrodes were applied: a silver palladium alloy developed specifically for PZT materials, fired-on at 1223 K, and an evaporated layer of chromium/gold. Little difference was found between the dielectric properties obtained using the two types but the chromium/gold was a simpler deposition method and was used for this study.

2.3. Electrical measurements

Dielectric properties were measured using an HP4092A impedance analyser over a frequency range of 10 Hz to 1 MHz whilst the temperature was varied from ambient to 573 K at a controlled rate of 2 K/min during heating.

Resistivity measurements were made under vacuum using a Keithley 6517 electrometer. At a controlled temperature a bias voltage of 15 V was applied to the material and the current drawn measured (Fig. 1). The initial current flow is dominated by the charging of the sample, and the speed of settling to a constant value is determined by the RC time constant of the measurement system. For this reason the resistivity was calculated from the value of current measured after 1000 s. Measurements of resistivity were made over a range of temperatures from ambient to 358 K.

Poling of the samples was accomplished by heating in oil to approximately 400 K, applying a dc field of 3 V/μm for 10 min and cooling to room temperature under bias.

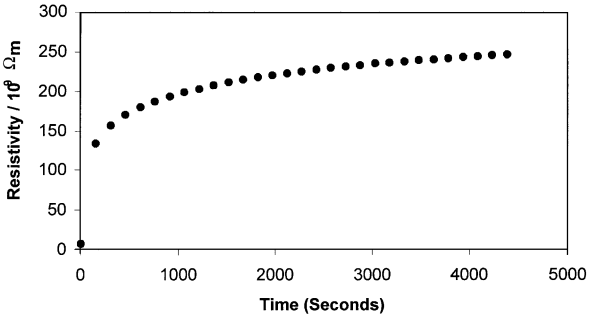

Fig. 1. Resistivity vs time plot for undoped composition (PZT–PMN).

Before pyroelectric measurements were made, samples were placed in an oven for 12 h at 323 K with the electrodes shorted out, to eliminate any space charges that had developed during poling.

Pyroelectric properties were measured by the Byer and Roundy method.[19] To make the measurement, the sample was contained within an evacuated chamber to ensure that the ambient humidity did not affect the results. The sample was heated and cooled at a constant rate by a computer controlled Peltier heater/cooler. A Keithley 6517 electrometer was used to measure the resulting pyroelectric current. This pyroelectric current can be related to the pyroelectric coefficient by the following equation:

$$I = Ap(T)\frac{\mathrm{d}T}{\mathrm{d}t} \tag{3}$$

For accurate results the measurement technique requires all the current to flow through the electrometer, although in practice, a small amount of current will flow through the sample. Byer and Roundy[19] have shown that the resistance of the sample needs to be at least 100 times the resistance of the electrometer for the errors to be below 1%. The resistances of the samples with the two highest levels of uranium doping were too low to achieve reliable results with this method and the electrometer available.

3. Results and discussion

Dielectric, pyroelectric and resistivity measurements are presented in Table 1. As the doping level of U_3O_8 was increased there was a rise in both the room temperature relative permittivity and the dielectric loss. Increases in loss were probably also brought about by the higher dc conductivity. Dielectric properties after poling exhibited the same trend. For the detector design it would be preferable for the relative permittivity at room temperature to decrease with doping, as it would lead to improved figures of merit, F_V and F_D.

Fig. 2 shows the resistivity (ρ) values measured as a function of temperature for the different uranium doping levels plotted as ρ against T^{-1}. The resistivity of the material was very sensitive to the doping level. The addition of 1 mol/% of uranium decreased the material's resistivity by approximately three orders of magnitude by comparison with the undoped material.[15]

It is clear from Fig. 2 that the variation of resistivity with temperature follows a power law of the form:

$$\rho = \rho_0 \exp(E_a/KT) \tag{4}$$

where E_a is the activation energy for the conduction process and ρ_0 a constant. The coefficients for the data presented in Fig. 2 are given in Table 2.

Table 1
Dielectric and pyroelectric measurements on U^{6+} doped PZT–PMN ceramics at 298 K[a]

Doping level of U^{6+} ($z\times100$)	Resistivity 10^8 Ωm	Relative permittivity (400 Hz)		tanδ/%		Pyroelectric coefficient 10^{-4} Cm^{-2} K^{-1}	F_v 10^{-2} m^2 C^{-1}	F_D 10^{-4} $Pa^{-0.5}$
		Pre-poling	Post-poling	Pre-poling	Post-poling			
0.48	122	283	220	0.81	0.30	2.8	5.8	4.7
0.59	38.1	290	207	0.76	0.43	3.0	6.6	4.3
0.77	8.58	286	215	0.99	0.80	2.7	5.6	2.7
1.1	2.26	353	281	2.08	2.08			
1.45	1.02	405	308	4.14	4.39			

[a] Specific heat capacity of PZT taken as 2.5 MJ m^{-3} K^{-1}.

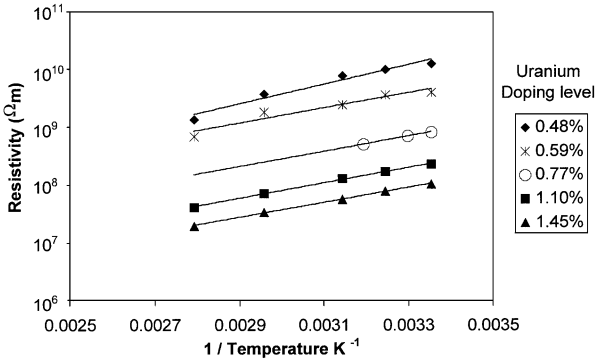

Fig. 2. Resistivity vs temperature for various uranium doping levels.

Table 2
Activation energies and ρ_0 for different levels of uranium doping

mol%[a] U^{6+}	E_a/eV	$\rho_0/10^3$ Ωm
0.48	0.34	26.4
0.59	0.28	77.5
0.77	0.26	31.0
1.1	0.26	8.22
1.45	0.26	5.04

[a] $z\times100$.

The difference in activation energy between the lowest doping levels and the highest is unlikely to be significant. Earlier work by Dih and Fulrath[20] has shown that relatively small changes in composition can give quite large changes in activation energy. They reported that for $PbZr_{0.5}Ti_{0.5}O_3$ doped with 2 mol% Nb_2O_5 the activation energy was 1.4 eV while a similar doping level of Sc_2O_3 gave an activation energy of 1.1 eV. The mean activation energy for the conduction process is estimated to be 0.28 ± 0.04 eV.

The values of activation energy found here are only slightly lower than those (0.37 ± 0.01 eV) reported previously[10,11] for similar uranium doping levels, where it was reasoned that the conduction mechanism in this range of uranium doping was by electron hopping. Whatmore[11] has previously discussed two possible mechanisms that could determine the change in conduction with uranium doping.

In the first mechanism charge carriers overcome the potential barriers at the grain boundaries. If the dopant ions were all fully ionised and the conduction dominated by carriers hopping over a potential barrier at the grain boundary, then it would be expected that the conductivity would be independent of the distance between the donor centres. As a consequence, the conductivity would be proportional to the doping level. Such a relationship was not found for the data from this study.

In the second mechanism conductivity is controlled by the activation energy for thermally-activated hopping conduction between carrier trapping sites within the crystal lattice of the ceramic grains. In this case the probability of a charge carrier hopping between two sites separated by a distance R due to the absorption of a phonon would be proportional to:

$$\upsilon\exp(-\alpha R) \tag{5}$$

where α is a constant at constant temperature and ν is a factor dependent upon phonon frequencies.

If the trapping sites are located at the dopant ions, as would be expected if the dopants were not ionised, then R is determined by the uranium oxide doping level, such that:

$$R = z^{-1/3}a \tag{6}$$

where a is the lattice parameter.

Then for electron hopping conduction the dc conductivity (σ_0) should be given by:

$$\sigma_0 = \mathrm{A}\exp(-\alpha a z^{-1/3} - E_a/\mathrm{kT}) \tag{7}$$

where A is a constant.

Plotting σ_o against $z^{-1/3}$ (Fig. 3) for the 298 K data from this study gives a similar graph to that reported for the PZ–PT–PFN system by Whatmore.[11] Fig. 3 also plots the data from this earlier study on the uranium-doped PZ–PT–PFN system, for the purposes of comparison. Exponential fits for the two data sets are shown superimposed on the graph. The equations for these lines are $y = 0.0005e^{-2.61x}$ for the uranium-doped PMN–PZT and $y = 0.0011e^{-2.71x}$ for PZ–PT–PFN, respectively.

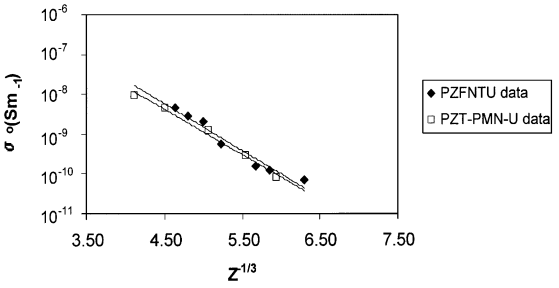

Fig. 3. Variation in conductivity with different doping levels of uranium (PZFNTU data from Refs. 10 and 11).

Table 3
Predicted vs actual resistivity of additional compositions

Mol% U^{6+}	Resistivity/10^8 Ωm	
	Intended	Actual
0.58	40.0	47.8
0.67	20.0	19.3
0.78	10.0	9.8

As the lattice parameter of the base composition is 4.142 Å this yields a value for α of 0.63 $Å^{-1}$, which is very similar to the value of 0.66 $Å^{-1}$ reported for PZ–PT–PFN.[11] This result strongly suggests that the conduction mechanism is primarily dominated by the position and number of uranium atoms on the lattice and is not related to the composition of the solid solution system. It would be expected, therefore, that a very similar result would be obtained whatever the base composition of PZT used.

Using the relationship derived from Fig. 3, three further compositions were prepared with the aim of achieving specific resistivities. Table 3 shows the measured and predicted values. Two compositions gave values within 3% of the predicted levels, confirming the validity of the model and illustrating its usefulness as a predictive tool.

3.1. Pyroelectric properties

The pyroelectric coefficients obtained varied between 2.7 and 3×10^{-4} Cm^{-2} K^{-1} for $z=0.0048$ to 0.0077 mol%, as shown in Table 1. The corresponding figures-of-merit are $F_V=0.066$ m^2C^{-1} and $F_D=4.7\times10^{-5}$ $Pa^{-1/2}$ at $z=0.006$. These values compare well with the values reported for the uranium-doped PZFNT system,[10] for which values of $F_V=0.04$ to 0.07 m^2 C^{-1} and $F_D=4$ to 6×10^{-5} $Pa^{-1/2}$ are typical.

4. Conclusions

It has been successfully demonstrated that the resistivity of a pyroelectric ceramic in the PZ–PT–PMN system can be controlled over several orders of magnitude by U_3O_8 doping. The variation of conductivity with uranium doping level has been shown to be very similar to that described previously in the PZT–PFN solid solution system.[11] This implies a similar conduction mechanism in both systems, probably electron hopping between U^{6+} ions on the B sites of the crystal lattice. Pyroelectric figures-of-merit were maintained over a wide range of doping levels, although there is evidence that high dopant levels decrease the figures of merit. However, it is unlikely that the material would be used in such a conductive form.

Acknowledgements

The work reported here has been supported financially by an EPSRC grant GR/L91436. R.W.W. gratefully acknowledges the financial support of the Royal Academy of Engineering. Thanks are also due to InfraRed Integrated Systems Ltd for financial support and to Dr. Chris Carter at that company for helpful discussions.

References

1. Putley, E. H., The pyroelectric detector. In *Semiconductors and Semimetals,* Vol. 5, ed. R. K. Willardson and A. C. Beer. Academic, New York, 1970, pp. 259–285.
2. Whatmore, R. W., Pyroelectric devices and materials. *Rep. Prog. Phys.,* 1986, **49**, 1335–1386.
3. Whatmore, R. W. and Watton, R., Pyroelectric devices and materials. In *Infrared Detectors and Emitters: Materials and Devices,* ed. P. Capper and C. T. Elliott. Kluwer Academic Publishers, 2000, pp. 99–147.
4. Watton, R., Pyroelectric materials: operation and performance in thermal imaging camera tubes and detector arrays. *Ferroelectrics,* 1976, **10**, 91.
5. Liu, S. T. and Long, D., Pyroelectric detectors and materials. *Proc. IEEE,* 1978, **66**, 14.
6. Berlincourt, D., Current developments in piezoelectric applications of ferroelectrics. *Ferroelectrics,* 1976, **10**, 111–119.
7. Whatmore, R. W., Pyroelectric ceramics and devices for thermal infra-red detection and imaging. *Ferroelectrics,* 1991, **118**, 241–259.
8. Bell, A. J. and Whatmore, R. W., Electrical conductivity in uranium-doped modified lead zirconate pyroelectric ceramics. *Ferroelectrics,* 1981, **37**, 543–546.
9. Whatmore, R. W. and Bell, A. J., Pyroelectric ceramics in the lead zirconate–lead titanate–lead iron niobate System. *Ferroelectrics,* 1981, **35**, 155–160.
10. Whatmore, R. W. and Ainger, F. W., Pyroelectric ceramic materials for uncooled infra-red detectors. In *Advances in Infra-Red Sensor Technology*, Vol. 395, ed. J. Besson. Proc. SPIE, 1983, pp. 261–266.
11. Whatmore, R. W., High performance conducting pyroelectric ceramics. *Ferroelectrics,* 1983, **49**, 201–210.
12. Kulscar, F., US Patent 3,006,857, 1961.
13. Ouchi, H., Nagano, K. and Hayakawa, S., Piezoelectric properties of $Pb(Mg_{1/3}Nb_{2/3})O_3$–$PbTiO_3$–$PbZrO_3$ solid solution ceramics. *J. Am. Ceram. Soc.,* 1965, **48**(12), 630–635.
14. Ouchi, H., Nishida, M. and Hayakawa, S., Piezoelectric properties of $Pb(Mg_{1/3}Nb_{2/3})O_3$–$PbTiO_3$–$PbZrO_3$ ceramics modified with certain additives. *J. Am. Ceram. Soc.,* 1966, **49**(11), 577–582.

15. Choi, S. W., Jang, S. J. and Bhalla, A., Dielectric properties in the $Pb(Mg_{1/3}Nb_{2/3})O_3$–$PbTiO_3$ solid solution system. *J. Korean Physical Society,* 1989, **22**(1), 91–96.
16. Shaw, C., Gupta, S., Stringfellow, S. B., Navarro, A., Alcock, J. R. and Whatmore, R. W., Pyroelectric properties of Mn-doped lead zirconate–lead titanate–lead magnesium niobate ceramics. Submitted to *J. Eur. Ceram. Soc.*
17. Swartz, S. L. and Shrout, T. R., Fabrication of perovskite lead magnesium niobate. *Mater. Res. Bull.,* 1982, **17**, 1245–1250.
18. Butcher, S. J. and Daglish, M., The use of magnesium carbonate hydroxide pentahydrate in the production of perovskite lead magnesium niobate. In *Proc. Third Euro-Ceramics*, Vol. 2, ed. P. Duran and J. F. Fernandez. Faenza Editrice Iberica SL, 1993, pp 121–126.
19. Byer, R. L. and Roundy, C. B., Pyroelectric coefficient direct measurement technique and application to nsec response time detector. *Ferroelectrics,* 1972, **3**, 333–338.
20. Dih, J. J. and Fulrath, R. M., Electrical conductivity in lead zirconate–titanate ceramics. *J. Am. Ceram. Soc.,* 1968, **61**(9–10), 448–451.